

Admittance and Impedance Representations of Friction Based on Implicit Euler Integration

Ryo Kikuuwe, *Member, IEEE*, Naoyuki Takesue, *Member, IEEE*, Akihito Sano, Hiromi Mochiyama, *Member, IEEE*, and Hideo Fujimoto

Abstract—Modeling of friction force is cumbersome because of its discontinuity at zero velocity. This paper presents a set of discrete-time friction models for the purpose of haptic rendering and virtual environment construction. These models allow friction to be treated as an admittance-type or impedance-type element of a virtual environment. They are derived from implicit Euler integration of Coulomb-like discontinuous friction and linear mass-spring-damper dynamics, and have closed-form expressions. They include rate-dependent friction laws, and their extension to multidimensional cases is easy in most practical cases. The validity of the models is demonstrated through numerical examples and implementation experiments.

Index Terms—Admittance, friction, haptic rendering, impedance, implicit Euler scheme.

I. INTRODUCTION

MODELING of friction force is important for realistic haptic interaction in virtual environments. In conventional models of friction, the friction force always opposes the velocity in kinetic friction, and when the velocity is zero (i.e., in static friction), the friction force acts to balance the other forces to maintain zero velocity. This property is cumbersome to simulate in discrete time. One reason is that the zero velocity, which triggers a transition to static friction, does not occur in discrete time. Another reason is that the definition of the friction force is different between kinetic friction and static friction. Conventional friction models suffer from chattering or unbounded drift in discrete time.

A virtual environment for haptic interaction can be described as a network of elements that represent various dynamic relations between motion and force. For extensible construction of virtual environments, it is desirable that every single element accepts either of velocity or force as an input and to produce the other as an output. An element that accepts a force input to produce a velocity output is called an admittance, while an element that accepts a velocity input to produce a force output is called an impedance. The conventional Coulomb friction model cannot be classified as either of these two types; in kinetic friction, it acts as an impedance which maps a velocity into a force

of opposite direction, while in static friction, it behaves as an admittance which maps an external force into the zero velocity. Some recent friction models have impedance-type formulations, but they suffer from unbounded drift or numerical stiffness, or have difficulties in extensibility to multidimensional cases.

This paper presents a set of discrete-time friction models of the admittance and impedance types. These friction models are derived based on implicit Euler integration of Coulomb-like discontinuous friction and linear mass-spring-damper dynamics. They do not exhibit drift or chattering. They have closed-form expressions, and thus they are suitable for realtime, fixed-step computation. They include rate-dependent friction laws, and can be extended to include multidimensional cases in most practical cases.

The rest of this paper is organized as follows. Section II provides an overview of previous approaches of friction modeling. Section III presents new friction models, and Section IV discusses suitable applications for each model. In Section V, the proposed models are demonstrated using haptic interfaces. Section VI provides the concluding remarks.

II. PREVIOUS APPROACHES

A. Conventional Models

Let us consider a rigid object that is in contact with a fixed surface and is moving at a velocity v with respect to the fixed surface. Let f be the friction force and h be the net force acting on the object from all other sources. The sign of f is chosen opposite to those of v and h . In conventional friction models, the friction force f is described as follows:

$$f = \begin{cases} \Phi(v), & \text{if } v \neq 0 \\ \Phi(+0), & \text{if } v = 0 \wedge h > \Phi(+0) \\ h, & \text{if } v = 0 \wedge h \in [\Phi(-0), \Phi(+0)] \\ \Phi(-0), & \text{if } v = 0 \wedge h < \Phi(-0). \end{cases} \quad (1)$$

Here, $\Phi(v)$ is a function that is continuous for all $v \neq 0$, satisfies $\Phi(v)v > 0$ for all $v \neq 0$, and has limits as $v \rightarrow +0$ and $v \rightarrow -0$. We write $\Phi(+0) = \lim_{v \rightarrow +0} \Phi(v)$ and $\Phi(-0) = \lim_{v \rightarrow -0} \Phi(v)$. Because of $\Phi(v)v > 0$, $\Phi(-0) < 0 < \Phi(+0)$ is satisfied. We use the function $\Phi(\cdot)$ to allow rate-dependent friction laws such as viscous effect. The stiction (static friction larger than kinetic friction) can be included in (1) by using a function $\Phi(v)$ having a large absolute value when v is around zero. In the case of Coulomb friction, the function $\Phi(\cdot)$ takes the simplest form, as follows:

$$\Phi(v) = F \operatorname{sgn}(v) \quad (2)$$

Manuscript received December 20, 2005; revised May 30, 2006. This paper was recommended for publication by Associate Editor D. Prattichizzo and Editors I. Walker and K. Lynch upon evaluation of the reviewers' comments. This paper was presented in part at the IEEE/RSJ International Conference on Intelligent Robots and Systems, Edmonton, AB, Canada, August 2005.

The authors are with the Department of Mechanical Engineering, Nagoya Institute of Technology, Nagoya 466-8555, Japan (e-mail: kikuuwe@nitech.ac.jp).

Digital Object Identifier 10.1109/TRO.2006.886262

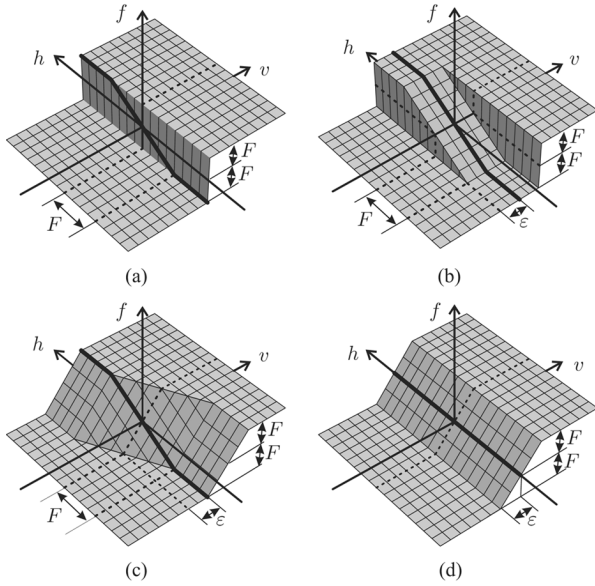


Fig. 1. Friction force f as a function of velocity v and external force h . (a) Coulomb friction model, defined by (1) and (2). (b) Karnopp's model [2], defined by (3) and (2). (c) Quinn's model [6], defined by (4). (d) Viscosity approximation [7], defined by (5). The thick black lines represent the value of f at $v = 0$.

where $F > 0$ is called the kinetic friction force. Fig. 1(a) shows a plot of (1) with the function $\Phi(\cdot)$ defined as (2). Difficulty in using the model (1) in digital computation is rooted in its discontinuity and singularity at $v = 0$. The friction force f is discontinuous with respect to v at $v = 0$, and is dependent on h exclusively when $v = 0$.

The exact zero velocity does not occur in discrete time. A conventional approach to realize static friction in discrete time is to use a threshold velocity below which the velocity is considered zero. This approach, which was presented by Karnopp [2], can be described as follows:

$$f = \begin{cases} \Phi(v), & \text{if } |v| > \varepsilon \\ \Phi(+0), & \text{if } |v| \leq \varepsilon \wedge h > \Phi(+0) \\ h, & \text{if } |v| \leq \varepsilon \wedge h \in [\Phi(-0), \Phi(+0)] \\ \Phi(-0), & \text{if } |v| \leq \varepsilon \wedge h < \Phi(-0) \end{cases} \quad (3)$$

where ε is a small positive value below which the velocity is considered zero. A plot of (3) is shown in Fig. 1(b). This approach has been widely used in haptic rendering [3], [4], but the behavior of the system is strongly influenced by the choice of ε value [5]. Moreover, the threshold ε cannot hold any physical meanings.

In order to remove the discontinuities in (3), Quinn [6] proposed the model equivalent to the following:

$$f = \begin{cases} F \text{sgn}(q), & \text{if } |q| > \varepsilon \\ Fq/\varepsilon, & \text{if } |q| \leq \varepsilon \end{cases} \quad (4a)$$

where q is the amount that is defined as

$$q = \begin{cases} v + \varepsilon \text{sgn}(h), & \text{if } |h| > F \\ v + \varepsilon h/F, & \text{if } |h| \leq F. \end{cases} \quad (4b)$$

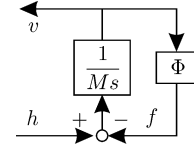


Fig. 2. Closed-loop system including an incomplete impedance element $\Phi(\cdot)$.

This model is illustrated in Fig. 1(c). Its behavior is also influenced by the value ε . Inclusion of rate-dependent friction laws [i.e., arbitrary function $\Phi(\cdot)$] is not addressed in Quinn's paper.

The models (3) and (4), which are dependent on the external force h , are classified as neither impedance nor admittance. The dependence on h can be removed by approximating the friction by a very high viscosity in a small velocity region [7]. This approach can be described as follows:

$$f = \begin{cases} F \text{sgn}(v), & \text{if } |v| > \varepsilon \\ Fv/\varepsilon, & \text{if } |v| \leq \varepsilon. \end{cases} \quad (5)$$

As illustrated in Fig. 1(d), this model is different from the original continuous-time expression (1) at $v = 0$. That is, the friction force does not balance the external force h at $v = 0$.

The above discrete-time models (3), (4), and (5), suffer from either drift or chattering, depending on the choice of the non-physical threshold ε . These undesirable behaviors can be removed by using a finite-state machine based on the detection of zero-velocity crossings (i.e., velocity reversals) [8], [9]. This approach, however, is not suitable for multidimensional systems [9], because velocity reversals cannot be defined strictly in multidimensional space. Adaptive timestep approaches for accurate zero-crossing detections are not suitable for realtime computation for haptic rendering.

In a strict sense, the dependence of (1) on the external force h is physically impossible. In continuous time, even the definition

$$f = \Phi(v) \quad (6)$$

is adequate to describe static friction, because the friction force f is switched infinitely fast around $v = 0$, and thus, apparently balances the external force h . Let us write the equation of motion of the sliding object as follows:

$$M\dot{v} = h - f \quad (7)$$

where M is the mass of the object. Then, (7) acts as a negative feedback loop enclosing the element $\Phi(\cdot)$, as shown in Fig. 2. In the neighborhood of $v = 0$, f is switched infinitely fast between $\Phi(+0) > 0$ and $\Phi(-0) < 0$, and thus v is constrained to be zero as long as $h \in [\Phi(-0), \Phi(+0)]$. This state can be viewed as a sliding mode [10] on the hypersurface $v = 0$ in the mathematical sense (though the mass is not sliding, but is in static friction in the physical sense). The element $\Phi(\cdot)$ can be viewed as an "incomplete" impedance element in the sense that its output is not defined for a zero input velocity. On the other hand, the system of Fig. 2 acts as an admittance-type system, which allows the

zero velocity as a sliding mode (in the mathematical sense). A sliding mode, however, does not occur in discrete time.

B. Impedance-Type Models

To formulate friction as an impedance-type element, nonzero velocity must be allowed as input even in static friction. Thus, an impedance-type friction model must exhibit elastic displacement in static friction. This displacement, which is termed as presliding displacement, exists also in real mechanical systems [11]. It usually has nonlinearity and hysteresis, and transitions between static and kinetic friction are usually ambiguous.

Some recent friction models attempt to capture features of real friction phenomena [12]–[17]. These models have continuous-time expressions based on differential equations. They all have one or more limitations in application to haptic rendering: unbounded drift, numerical stiffness, or difficulty in extension to multidimensional cases. Drift has been removed from most recent models [12]–[17]. Ferretti *et al.*'s integral friction model [17] is numerically robust, being accurate even with Euler integration. However, extension to multidimensional cases is commonly difficult, even in these models. A practical remedy is to determine each component of the friction force vector separately according to the corresponding component of the velocity vector, as in [18]. This approach, however, makes the system variant to the coordinate transformations. A multidimensional version of LuGre model has been derived [19], but the drift characteristic of LuGre model [13] is not eliminated.

Another group of impedance-type friction models exhibit simple linear elasticity in static friction. In Haessig and Friedland's reset integrator model [20], the input velocity is integrated into the elastic displacement as long as it does not exceed a predetermined saturation level. This model enters kinetic friction state when the elastic displacement reaches the saturation level. This model includes viscous damping only under static friction. Thus, there must be a discontinuity at a transition from static friction to kinetic friction. Simpler models including linear elasticity without viscous damping have been used for the purposes of haptic rendering and physics-based animations. In Hayward and Armstrong's model [21], a virtual object on a surface is connected to a haptic interface via a virtual spring. The spring is allowed to extend up to a predetermined length, and when it is exceeded, the virtual object starts to slide. Similar models have been used for simulating friction between two virtual objects [22], [23]. Such approaches can be classified as a penalty-based approach [23], in which "forbidden" configurations (such as penetration between objects and displacement during sticking) are penalized by virtual spring forces. A drawback of such models is that they are prone to oscillations in static friction, since they include no damping. Moreover, there are no coherent algorithms to determine the spring length under rate-dependent friction laws.

C. Constraint-Based Models

As a middle way between (1) and (6), we can consider the following expression:

$$f \begin{cases} = \Phi(v), & \text{if } v \neq 0 \\ \in [\Phi(-0), \Phi(+0)], & \text{if } v = 0 \end{cases} \quad (8)$$

or equivalently

$$(f = \Phi(v) \wedge v \neq 0) \vee (f \in [\Phi(-0), \Phi(+0)] \wedge v = 0). \quad (9)$$

A similar expression has been used [24] for modeling relay systems such as Coulomb friction. This expression describes an algebraic constraint between the friction force f and the velocity v at a given instant. This type of approach can be used in constraint-based simulations [23], in which state variables are determined so as to satisfy given constraints. The advantage of this approach is accuracy, without chattering or drift, in simulating rigid-body dynamics including Coulomb friction. However, this approach does not usually provide closed-form analytical solutions.

III. NEW FRICTION MODELS

In this section, we derive four discrete-time friction models, two being the admittance type and the other two being the impedance type. They are related in a circular manner, as illustrated in Fig. 3. The model A (rigid admittance model) and the model C (massless impedance model) are special cases of the model D (compliant admittance model) and the model B (inertial impedance model), respectively. We, however, treat them separately, because the special models have different discrete-time representations from the general models. Among the four models, the models A and C will be practically useful for the purposes of haptic rendering and penalty-based simulations. The models B and D can be effective in some limited cases to maintain numerical stability. The strength of each model is discussed later in Section IV.

In each model, the incomplete impedance element $\Phi(\cdot)$ is enclosed in a closed feedback loop. Discrete-time representations of these models are derived by using the implicit Euler scheme, so that the input and output of the element $\Phi(\cdot)$ are algebraically constrained. In this sense, this approach can be viewed as a "locally" constraint-based approach, and as a result, chattering and drift are removed. The discrete-time representations of the models include analytical solutions (or closed-form approximations of the solutions) for the algebraic constraints. The implicit Euler approach has been applied to simulate relay systems (including Coulomb friction) [25], but there have been no attempts to formulate friction as an element with a closed-form expression.

We start our derivation from the model A, which represents a rigid sliding mass. The other models are derived in the order indicated in Fig. 3. Through the derivation of the model A in Section III-A, we introduce some basic mathematical operations to treat the discontinuous function $\Phi(\cdot)$ in discrete time. Similar operations are used to derive the other three models, through Section III-B to III-D. Section III-E discusses a closed-form approximation for the models in case where an analytical solution cannot be obtained. Section III-F discusses extension to multidimensional space. For brevity of description, we assume that $f = \Phi(v)$ implies (9) throughout the rest of this paper. That is, we assume that $f = \Phi(0)$ means $f \in [\Phi(-0), \Phi(+0)]$.

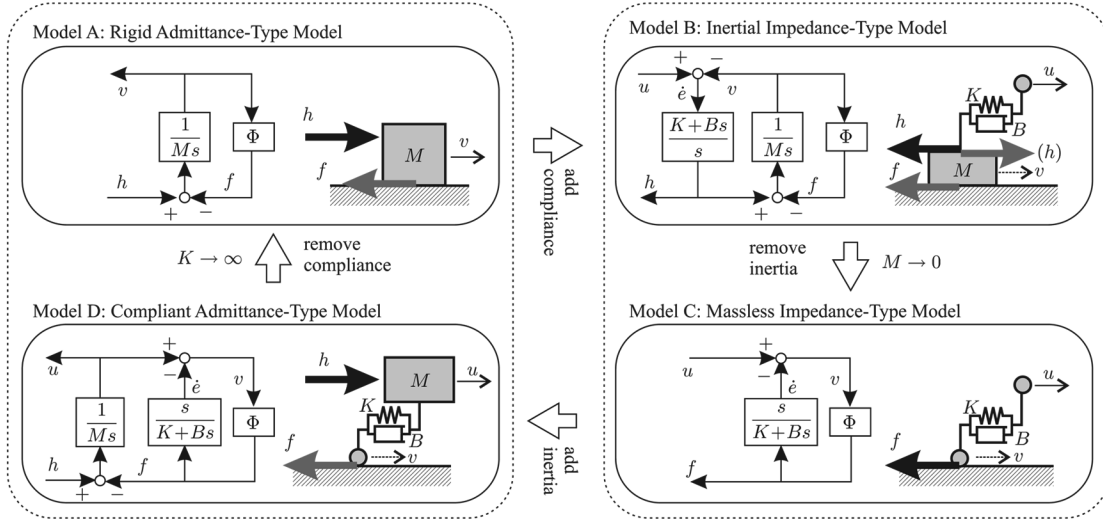


Fig. 3. Four types of friction model. The discrete-time representations of the models A, B, C, and D are (26), (36), (38), and (45), respectively.

A. Model A: Rigid Admittance-Type Model

The model A, the rigid admittance-type model, represents a rigid object sliding on a fixed surface. This system contains two constraints

$$M\dot{v} = h - f \quad (10)$$

$$f = \Phi(v) \quad (11)$$

where M is the mass of the object. A discrete-time approximation of (10) based on the Euler scheme is written as follows:

$$M(v_k - v_{k-1})/T = h_k - f_k \quad (12)$$

where T denotes the timestep size and the subscripts denote the time indices. In the explicit (forward) Euler method, the current friction force f_k is determined so as to satisfy $f_k \approx \Phi(v_{k-1})$ because, in (12), v_k can be determined only after f_k is determined. Instead of this, we consider using

$$f_k = \Phi(v_k). \quad (13)$$

In (12) and (13), v_k and f_k are mutually dependent. Therefore, in order to obtain v_k and f_k , we have to solve (12) and (13) as a pair of algebraic equations. This kind of approach is known as the implicit (backward) Euler method.

We attempt to derive an analytical solution for the system of (12) and (13). Eliminating v_k from (13) yields

$$f_k = \Phi(v_k^* - Tf_k/M) \quad (14)$$

where $v_k^* = v_{k-1} + Th_k/M$. Since v_k^* is known, (14) is an algebraic equation with unknown f_k . In order to solve this equation, we introduce the following theorem.

Theorem 1: Let x and y be real numbers and Z be a positive real number. Assume that the function $\Phi(\cdot)$:

- is continuous for all $x \neq 0$;
- satisfies $\Phi(x)x > 0$ for all $x \neq 0$;
- has limits as $x \rightarrow +0$ and $x \rightarrow -0$;

and satisfies

$$\Phi'(x) > -1/Z \quad \forall x \neq 0 \quad (15)$$

where $\Phi'(x) = d\Phi(x)/dx$. Define the function $\Phi_Z(\cdot)$ as shown in (16) at the bottom of the page. Then, the statement

$$y = \Phi(x - Zy) \iff y = \Phi_Z(x) \quad (17)$$

holds true.

Proof: Because $\Phi(x)$ is continuous in $x \in (-\infty, 0)$ and $x \in (0, \infty)$, the assumption (15) implies

$$\begin{aligned} \Phi(x) &< \Phi(-0) - x/Z \quad \forall x < 0 \\ \Phi(x) &> \Phi(+0) - x/Z \quad \forall x > 0 \end{aligned} \quad (18)$$

which is equivalent to

$$\Phi(x) + x/Z \notin [\Phi(-0), \Phi(+0)] \iff x \neq 0. \quad (19)$$

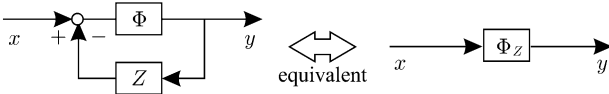
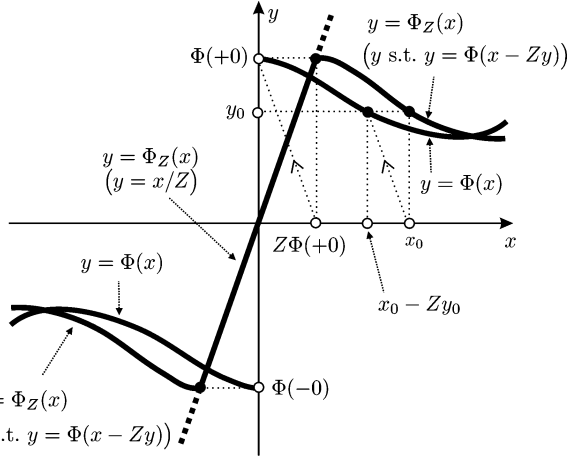
Substituting x in the above by $x - Zy$ yields

$$\Phi(x - Zy) + x/Z - y \notin [\Phi(-0), \Phi(+0)] \iff x - Zy \neq 0.$$

If $y = \Phi(x - Zy)$, the above can be rewritten as

$$x/Z \notin [\Phi(-0), \Phi(+0)] \iff x - Zy \neq 0. \quad (20)$$

$$\Phi_Z(x) = \begin{cases} y \text{ s.t. } y = \Phi(x - Zy), & \text{if } x/Z \notin [\Phi(-0), \Phi(+0)] \\ x/Z, & \text{if } x/Z \in [\Phi(-0), \Phi(+0)] \end{cases} \quad (16)$$

Fig. 4. Block-diagram representation of the relation between $\Phi(\cdot)$ and $\Phi_Z(\cdot)$.Fig. 5. Relation between $\Phi(\cdot)$ and $\Phi_Z(\cdot)$; x_0 is an arbitrary value, and y_0 is defined as $y_0 = \Phi_Z(x_0)$, which is equivalent to $y_0 = \Phi(x_0 - Zy_0)$.

The statement $y = \Phi(x - Zy)$ is equivalent to

$$\begin{aligned} & ((y = \Phi(x - Zy)) \wedge (x - Zy \neq 0)) \\ & \vee ((y \in [\Phi(-0), \Phi(+0)]) \wedge (x - Zy = 0)). \end{aligned} \quad (21)$$

Due to (20), the above can be rewritten as

$$\begin{aligned} & ((y = \Phi(x - Zy)) \wedge (x/Z \notin [\Phi(-0), \Phi(+0)])) \\ & \vee ((x/Z \in [\Phi(-0), \Phi(+0)]) \wedge (y = x/Z)) \end{aligned} \quad (22)$$

which is equivalent to the statement $y = \Phi_Z(x)$ where $\Phi_Z(\cdot)$ is defined by (16). Therefore, $y = \Phi_Z(x)$ is satisfied if $y = \Phi(x - Zy)$. The converse is trivial from (16). ■

Figs. 4 and 5 illustrate the relation between $\Phi(\cdot)$ and $\Phi_Z(\cdot)$. Although the nonlinear algebraic equation in (16) cannot generally be solved analytically, $\Phi_Z(\cdot)$ exists uniquely if (15) is satisfied. A closed-form approximation for $\Phi_Z(\cdot)$ in cases where an analytical solution is not obtained is discussed later in Section III-E. In some simple cases, the equation in (16) can be analytically solved. For example, in the case of Coulomb friction, $\Phi(\cdot)$ reduces to $\Phi(x) = F \text{sgn}(x)$, and its counterpart is

$$\Phi_Z(x) = \begin{cases} F \text{sgn}(x), & \text{if } |x| > ZF \\ x/Z, & \text{if } |x| \leq ZF. \end{cases} \quad (23)$$

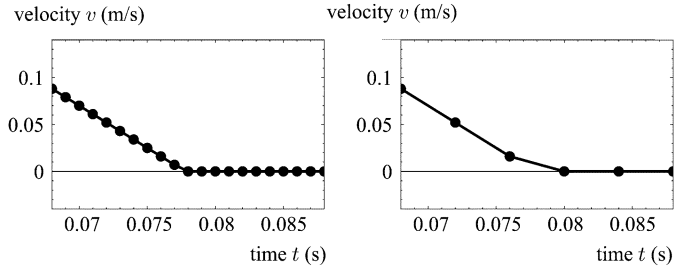
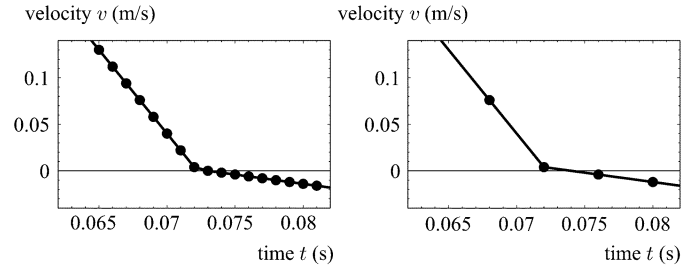
When a viscous effect is present, $\Phi(\cdot)$ becomes

$$\Phi(x) = F \text{sgn}(x) + Dx \quad (24)$$

and its counterpart is

$$\Phi_Z(x) = \begin{cases} (F \text{sgn}(x) + Dx)/(1 + ZD), & \text{if } |x| > ZF \\ x/Z, & \text{if } |x| \leq ZF \end{cases} \quad (25)$$

where $D > 0$ is the viscosity coefficient.

Fig. 6. Simulation of the model A exhibiting zero-velocity reaching; timestep size $T = 0.001$ s (left) and 0.004 s (right); initial condition $v = 0.7$ m/s and input $h = -1$ N; $M = 1$ kg, $\Phi(v) = F \text{sgn}(v)$, $F = 8$ N.Fig. 7. Simulation of the model A exhibiting a velocity reversal; timestep size $T = 0.001$ s (left) and 0.004 s (right); initial condition $v = 1.3$ m/s and input $h = -10$ N; $M = 1$ kg, $\Phi(v) = F \text{sgn}(v)$, $F = 8$ N.

Based on *Theorem 1*, the solution for (14) is written as $f_k = \Phi_{T/M}(v_k^*)$. In conclusion, the computational procedure of the model A is obtained as follows:

$$v_k^* := v_{k-1} + Th_k/M \quad (26a)$$

$$f_k := \Phi_{T/M}(v_k^*) \quad (26b)$$

$$v_k := v_k^* - Tf_k/M. \quad (26c)$$

This is the solution for the pair of algebraic equations (12) and (13). This new model (26) sets the velocity to be zero when $Mv_k^*/T \in [\Phi(-0), \Phi(+0)]$ is satisfied. Here, v_k^* can be interpreted as the velocity that could have been achieved if no friction force acted. It is straightforward to see that $|v_k| < |v_k^*|$ if $v_k^* \neq 0$, and that $v_k = 0$ if $v_k^* = 0$. This means that the friction force f_k always acts to decrease the kinetic energy. That is, this friction model is guaranteed to be dissipative regardless of the timestep size T .

Fig. 6 shows example results of a numerical simulation using this model. In this simulation, a rigid object ($M = 1$ kg) with a positive initial velocity ($v = 1.3$ m/s) is pulled with a negative constant force $h = -1$ N, which is smaller than the friction force $\Phi(v) = F \text{sgn}(v)$ where $F = 8$ N. The timestep size was chosen as $T = 0.001$ s in Fig. 6 (left) and $T = 0.004$ s in Fig. 6 (right). Fig. 6 shows that the object reaches the zero velocity without chattering, irrespective of the timestep size.

When the external force h is larger than the friction force, the velocity is reversed after crossing the zero velocity. Fig. 7 shows another set of simulation results exhibiting this behavior. The velocity may or may not reach the exact zero at the velocity reversal, but it is not a problem, because zero velocity occurs only for an infinitely short time period even in continuous time.

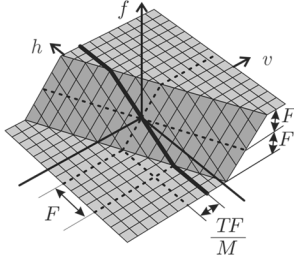


Fig. 8. Proposed model A, defined by (27).

This model can be compared with the conventional models overviewed in Fig. 1 in Section II-A. In the case of Coulomb friction, i.e., $\Phi(v) = F \text{sgn}(v)$, (26a) and (26b) reduce to (27), shown at the bottom of the page. A plot of (27) is shown in Fig. 8. This model is identical to the Coulomb friction model [Fig. 1(a)] at $v = 0$, and is simpler than Karnopp's model [Fig. 1(b)] and Quinn's model [Fig. 1(c)]. Unlike the conventional models, the model (27) includes no arbitrariness in threshold settings.

B. Model B: Inertial Impedance-Type Model

The model B, the inertial impedance-type model, is obtained by adding a compliance (spring-damper) element to the model A, as illustrated in Fig. 3. One end of the compliance element is connected to the sliding mass, and the other end is pulled with an input velocity u . Because the force produced by the compliance element corresponds to the force h , there is the following constraint among u , v , and h :

$$h = Ke + B\dot{e}, \quad e = \int (u - v) dt, \quad (28)$$

where K and B are the stiffness and viscosity of the compliance element, and e can be interpreted as the displacement due to the compliance element. A discrete-time approximation of (28) based on the Euler scheme is written as

$$h_k = Ke_k + B(e_k - e_{k-1})/T \quad (29)$$

$$(e_k - e_{k-1})/T = u_k - v_k. \quad (30)$$

Remember that the model A includes two constraints (12) and (13). In addition to them, the model B includes another constraint produced by (29) and (30). From (30), v_k is written as $v_k = u_k - (e_k - e_{k-1})/T$. By using this, we can eliminate v_k and v_{k-1} from (12) and (13), obtaining

$$\frac{M}{T} \left(u_k - u_{k-1} - \frac{e_k - 2e_{k-1} + e_{k-2}}{T} \right) = h_k - f_k \quad (31)$$

$$f_k = \Phi(u_k - (e_k - e_{k-1})/T). \quad (32)$$

Thus, we can conclude that the model B includes three algebraic constraints: (29), (31), and (32). The unknown variables of this set of equations are h_k , e_k , and f_k .

Eliminating h_k and e_k from (32) yields

$$f_k = \Phi(v_k^* - Tf_k/C) \quad (33)$$

where

$$v_k^* = u_k + \frac{TK}{C} e_{k-1} - \frac{M}{C} \left(u_k - u_{k-1} + \frac{e_{k-1} - e_{k-2}}{T} \right) \quad (34)$$

$$C = M + TB + T^2K. \quad (35)$$

From *Theorem 1*, the solution for the algebraic constraint (33) is obtained as $f_k = \Phi_{T/C}(v_k^*)$. Based on this, the other unknown variables, h_k and e_k , can be obtained by using (29) and (31). In conclusion, the computational procedure for solving the set of constraints (29), (31), and (32) is written as follows:

$$v_k^* := u_k + \frac{TK}{C} e_{k-1} - \frac{M}{C} \left(u_k - u_{k-1} + \frac{e_{k-1} - e_{k-2}}{T} \right) \quad (36a)$$

$$f_k := \Phi_{T/C}(v_k^*) \quad (36b)$$

$$e_k := e_{k-1} + Tu_k - T(v_k^* - Tf_k/C) \quad (36c)$$

$$h_k := Ke_k + B(e_k - e_{k-1})/T. \quad (36d)$$

Under the condition $Cv_k^*/T \in [\Phi(-0), \Phi(+0)]$, (36) reduces to

$$e_k := e_{k-1} + Tu_k \quad (37a)$$

$$h_k := Ke_k + B(e_k - e_{k-1})/T. \quad (37b)$$

This implies that, when $Cv_k^*/T \in [\Phi(-0), \Phi(+0)]$ is satisfied, the model B is in static friction, acting as a spring-damper element that produces the force h_k according to the input velocity u_k . This means that the model B does not exhibit drift under a small input velocity.

C. Model C: Massless Impedance-Type Model

The model C, massless impedance-type model, is the special case of the model B where $M = 0$. It is obtained by substituting (36) by $M = 0$ as follows:

$$v_k^* := u_k + Ke_{k-1}/(B + TK) \quad (38a)$$

$$f_k := \Phi_{1/(B+TK)}(v_k^*) \quad (38b)$$

$$e_k := (Be_{k-1} + Tf_k)/(B + TK). \quad (38c)$$

In this case, h_k in (36) reduces to be equal to f_k . Notice that the computational procedure (38) is the solution for the following set of constraints:

$$f_k = \Phi(u_k - (e_k - e_{k-1})/T) \quad (39)$$

$$f_k = Ke_k + B(e_k - e_{k-1})/T. \quad (40)$$

$$f_k = \begin{cases} F \text{sgn}(v_{k-1} + Th_k/M), & \text{if } |v_{k-1} + Th_k/M| > TF/M \\ Mv_{k-1}/T + h_k, & \text{if } |v_{k-1} + Th_k/M| \leq TF/M \end{cases} \quad (27)$$

This model does not exhibit drift under a small input velocity, as explained with regard to the model B. The model C is in static friction when $(B + TK)v_k^* \in [\Phi(-0), \Phi(+0)]$ is satisfied.

When we set $B = 0$ and $\Phi(v) = F\text{sgn}(v)$, the model C becomes equivalent to a special case of Hayward and Armstrong's model [21]. (A general version of their model includes creeping in static friction, which is not included in the model C.) An advantage of the model C is that it allows a nonzero viscous coefficient and rate-dependent friction laws. Especially, nonzero viscous coefficient is effective to suppress vibration in a haptic interface and objects in a virtual environment. The model C is different from Haessig and Friedland's reset integrator model [20] in that the model C includes viscous damping in a consistent manner across static friction and kinetic friction, even under rate-dependent friction laws.

D. Model D: Compliant Admittance-Type Model

The model D, the compliant admittance-type model, is obtained by adding a mass to the model C, as illustrated in Fig. 3. This additional mass M produces a constraint between u_k and f_k , which is described as

$$M(u_k - u_{k-1})/T = h_k - f_k \quad (41)$$

where h_k is the input force applied to the mass M . Thus, the model D includes three algebraic constraints: (39), (40), and (41). In this set of constraints, the unknown variables are u_k , e_k , and f_k . Eliminating u_k and e_k from (39) yields

$$f_k = \Phi(v_k^* - Af_k) \quad (42)$$

where

$$v_k^* = u_{k-1} + Th_k/M + Ke_{k-1}/(B + TK) \quad (43)$$

$$A = (T^2K + TB + M)/(M(B + TK)). \quad (44)$$

From *Theorem 1*, the solution for (42) is $f_k = \Phi_A(v_k^*)$. Thus, the computational procedure to solve the set of the three constraints (39), (40), and (41) is given as follows:

$$v_k^* := u_{k-1} + Th_k/M + Ke_{k-1}/(B + TK) \quad (45a)$$

$$f_k := \Phi_A(v_k^*) \quad (45b)$$

$$e_k := (Be_{k-1} + Tf_k)/(B + TK) \quad (45c)$$

$$u_k := u_{k-1} + T(h_k - f_k)/M. \quad (45d)$$

This model reduces to the model A, (26), with $K \rightarrow \infty$. This means that this model can be used even when the stiffness K is infinitely high. This model is in static friction when $v_k^*/A \in [\Phi(-0), \Phi(+0)]$ is satisfied.

E. Closed-Form Approximation of Implicit Function $\Phi_Z(\cdot)$

We have shown that the algebraic equation in (16) has analytical solutions in some simple cases. In cases where (16) cannot be solved, $\Phi_Z(x)$ must be properly approximated by a closed-form expression. Such approximations must be continuous for all x because any discontinuities can cause unrealistic

abrupt changes in the friction force during a smooth change in the velocity.

A simple approximation of $\Phi_Z(x)$ can be obtained by replacing $\Phi(x)$'s discontinuity by a linear function x/Z without changing the gross shape of $\Phi(x)$. This approximation is described as

$$\Phi_Z(x) \approx \hat{\Phi}_Z(x) \triangleq \begin{cases} \Phi(x), & \text{if } |x/Z| > |\Phi(x)| \\ x/Z, & \text{if } |x/Z| \leq |\Phi(x)|. \end{cases} \quad (46)$$

The error introduced by using the approximation (46) instead of (16) is

$$\begin{aligned} |\hat{\Phi}_Z(x) - \Phi_Z(x)| &= |\Phi(x) - \Phi(x - Z\Phi_Z(x))| \\ &= Z|\Phi_Z(x)\Phi'(x)| + O(Z^2) \end{aligned} \quad (47)$$

when $|x/Z| > |\Phi(x)|$ and $x/Z \notin [\Phi(-0), \Phi(+0)]$. This error can be considered small if

$$|\Phi'(x)| \ll 1/Z \quad \forall x \neq 0 \quad (48)$$

is satisfied, because substituting (47) by (48) yields $|\hat{\Phi}_Z(x) - \Phi_Z(x)| \ll |\Phi_Z(x)|$. That is, (48) is the condition for the validity of the approximation (46).

Let the solutions for $x/Z = \Phi(x)$ be $x = x_{+0} > 0$ and $x = x_{-0} < 0$. When the approximation (46) is used, the maximum static friction force becomes $\Phi(x_{+0})$ and $\Phi(x_{-0})$, which are different from the correct values, $\Phi(+0)$ and $\Phi(-0)$. The difference between $\Phi(x_{+0})$ and $\Phi(+0)$ is

$$\begin{aligned} |\Phi(x_{+0}) - \Phi(+0)| &= |\Phi'(x_{+0})x_{+0}| + O(x_{+0}^2) \\ &= Z|\Phi(x_{+0})\Phi'(x_{+0})| + O(Z^2). \end{aligned} \quad (49)$$

If the condition (48) holds, this difference can also be considered small, because substituting (49) by (48) yields $|\Phi(x_{+0}) - \Phi(+0)| \ll |\Phi(x_{+0})|$. In the same way, we have $|\Phi(x_{-0}) - \Phi(-0)| \ll |\Phi(x_{-0})|$. Therefore, the error in maximum static friction force introduced by the approximation (46) can also be considered small if the condition (48) is satisfied.

Note that (48) is a stronger condition than (15), which is the condition for the existence of $\Phi_Z(\cdot)$. The constant Z is defined as $Z = T/M$, $Z = T/C$, $Z = 1/(B + TK)$, and $Z = A$ in the models A, B, C, and D, respectively. Thus, the condition (48) has to be considered in choosing the parameter values in the models.

F. Multidimensional Representations

We consider extensions of the proposed models into multidimensional cases, in which velocities and forces are represented by vectors. Equations (26), (36), (38), and (45), which represent the models A, B, C, and D, respectively, can be used in n -dimensional cases by interpreting the variables (forces, velocities, and displacements, i.e., f , h , v , u , v^* , and e) as \mathcal{R}^n vectors and $\Phi_Z(\cdot)$ as a map from \mathcal{R}^n into \mathcal{R}^n . We limit our discussion to the case where the stiffness, viscosity, and inertia coefficients, K , B , M , respectively, are scalars. The problem to be discussed here is to find an n -dimensional version of $\Phi_Z(\cdot)$. (Remember that Z is also a scalar, which depends on K , B , M , and T .)

Let $\Phi(\cdot)$ be a map from a velocity vector ($\in \mathcal{R}^n$) to a friction force vector ($\in \mathcal{R}^n$). We assume that the map $\Phi(\mathbf{x})$ is continuous for all $\mathbf{x} \neq \mathbf{0}$, satisfies $\mathbf{x}^T \Phi(\mathbf{x}) > 0$ for all $\mathbf{x} \neq \mathbf{0}$, and has limits $\lim_{\varepsilon \rightarrow +0} \Phi(\varepsilon \mathbf{x})$ for all $\mathbf{x} \neq \mathbf{0}$. (Here, $\mathbf{x} \in \mathcal{R}^n$, and $\mathbf{0}$ is the zero vector of \mathcal{R}^n .) Hereafter, we write $\Phi(+0 \cdot \mathbf{x}) = \lim_{\varepsilon \rightarrow +0} \Phi(\varepsilon \mathbf{x})$. Let us define a set \mathcal{F} as follows:

$$\mathcal{F} = \{\mathbf{y} \in \mathcal{R}^n \mid \mathbf{y} = \kappa \Phi(+0 \cdot \mathbf{x}), \kappa \in [0, 1], \mathbf{x} \in \mathcal{R}^n\}. \quad (50)$$

Then, we can interpret \mathcal{F} as the set of possible friction forces at zero velocity, i.e., $\Phi(\mathbf{0}) \in \mathcal{F}$. That is, we can interpret the statement $\mathbf{f} = \Phi(\mathbf{v})(\mathbf{f}, \mathbf{v} \in \mathcal{R}^n)$ to imply

$$(\mathbf{f} = \Phi(\mathbf{v}) \wedge \mathbf{v} \neq \mathbf{0}) \vee (\mathbf{f} \in \mathcal{F} \wedge \mathbf{v} = \mathbf{0}) \quad (51)$$

which is an n -dimensional version of (9).

As a $\Phi(\cdot)$ has its correspondent $\Phi_Z(\cdot)$ as defined in (16), a $\Phi(\cdot)$ must have its correspondent $\Phi_Z(\cdot)$, which is also a map from \mathcal{R}^n into \mathcal{R}^n . The closed interval $[\Phi(-0), \Phi(+0)]$ in (16) corresponds to the set \mathcal{F} in n -dimensional space. Therefore, in the same way as (16), we can write an n -dimensional version of $\Phi_Z(\cdot)$ as follows:

$$\Phi_Z(\mathbf{x}) = \begin{cases} \mathbf{y} \text{ s.t. } \mathbf{y} = \Phi(\mathbf{x} - Z\mathbf{y}), & \text{if } \mathbf{x}/Z \notin \mathcal{F} \\ \mathbf{x}/Z, & \text{if } \mathbf{x}/Z \in \mathcal{F}. \end{cases} \quad (52)$$

As is the case with the expression (16), the above expression includes an implicit form.

This implicit form in (52) can be analytically solved in some simple cases. The simplest example is the case where $\Phi(\mathbf{x}) = F\mathbf{x}/\|\mathbf{x}\|$, which represents Coulomb friction force, where $F > 0$ is the kinetic friction force. In this case, \mathcal{F} reduces to $\mathcal{F} = \{\mathbf{y} \in \mathcal{R}^n \mid \|\mathbf{y}\| \leq F\}$, and its correspondent $\Phi_Z(\cdot)$ is written as

$$\Phi_Z(\mathbf{x}) = \begin{cases} F\mathbf{x}/\|\mathbf{x}\|, & \text{if } \|\mathbf{x}\| > ZF \\ \mathbf{x}/Z, & \text{if } \|\mathbf{x}\| \leq ZF. \end{cases} \quad (53)$$

When a viscous effect is present, $\Phi(\cdot)$ becomes

$$\Phi(\mathbf{x}) = F\mathbf{x}/\|\mathbf{x}\| + D\mathbf{x} \quad (54)$$

and its counterpart is

$$\Phi_Z(\mathbf{x}) = \begin{cases} (F\mathbf{x}/\|\mathbf{x}\| + D\mathbf{x})/(1 + ZD), & \text{if } \|\mathbf{x}\| > ZF \\ \mathbf{x}/Z, & \text{if } \|\mathbf{x}\| \leq ZF \end{cases} \quad (55)$$

where $D > 0$ is the viscous coefficient.

If the friction force is always in the direction opposite to the velocity, i.e., if $\|\mathbf{x}\| \|\Phi(\mathbf{x})\| = \mathbf{x}^T \Phi(\mathbf{x}) \forall \mathbf{x} \neq \mathbf{0}$, the discussion in the one-dimensional case can be directly applied. From *Theorem 1*, the implicit form in (52) has a unique solution when the following condition is satisfied:

$$(\partial \|\Phi(\mathbf{x})\| / \partial \mathbf{x})(\mathbf{x} / \|\mathbf{x}\|) > -1/Z \quad \forall \mathbf{x} \neq \mathbf{0} \quad (56)$$

which is an n -dimensional version of (15). An approximation for $\Phi_Z(\mathbf{x})$ can be obtained in the same manner as (46) in Section III-E, as follows:

$$\Phi_Z(\mathbf{x}) \approx \hat{\Phi}_Z(\mathbf{x}) \triangleq \begin{cases} \Phi(\mathbf{x}), & \text{if } \|\mathbf{x}/Z\| > \|\Phi(\mathbf{x})\| \\ \mathbf{x}/Z, & \text{if } \|\mathbf{x}/Z\| \leq \|\Phi(\mathbf{x})\|. \end{cases} \quad (57)$$

This approximation is valid under the condition that

$$|(\partial \|\Phi(\mathbf{x})\| / \partial \mathbf{x})(\mathbf{x} / \|\mathbf{x}\|)| \ll 1/Z \quad \forall \mathbf{x} \neq \mathbf{0} \quad (58)$$

which is an n -dimensional version of (48).

In the general case, the formulation given in (52) does not guarantee the existence and uniqueness of the solution $\Phi_Z(\cdot)$. However, adopting a generalization of (46), we can derive an approximation of $\Phi_Z(\mathbf{x})$ that is valid at least when $\mathbf{x} \gg Z\|\Phi(\mathbf{x})\|$ or $\mathbf{x} \approx \mathbf{0}$, as shown in (59) at the bottom of the page. This approximation is continuous for all \mathbf{x} and satisfies $\hat{\Phi}_Z(\mathbf{x}) \approx \Phi_Z(\mathbf{x})$ in $\|\mathbf{x}\| \gg Z\|\Phi(\mathbf{x})\|$, and $\hat{\Phi}_Z(\mathbf{x}) = \Phi_Z(\mathbf{x})$ in $\mathbf{x} \approx \mathbf{0}$. Although the accuracy and validity of such an approximation are not demonstrated here, this choice of $\hat{\Phi}_Z(\cdot)$ in (59) can be considered in cases when analytical solutions or more valid approximations cannot be obtained.

Hayward and Armstrong's model [21] also has a multidimensional version. Aside from its inclusion of creeping behavior, their multidimensional model can be considered as a special case of the multidimensional model C because our model allows nonzero viscous coefficient B and rate-dependent friction laws.

IV. DISCUSSIONS

A. Versatility of Model C

The scope of application of the models A, B, and D is limited because they cannot deal with the case where a single object has more than one frictional contact. The model C, on the other hand, can be used as a versatile element representing a single frictional interface, because this model is a local model dependent only on the relative velocity, being separated from the dynamics of objects. Fig. 9 shows a simple example of multiple frictional contacts, which is also introduced in [6]. Fig. 10 shows an application of the model C for simulating the system of Fig. 9. Results of this simulation are presented in Fig. 11, in which realistic stick-slip oscillations are properly demonstrated in both frictional contacts.

B. Strength of Models B and D

The models B and D contain both mass and compliance, while the models A and C contain only one of mass and compliance. Thus, one may think that the models B and D can be decomposed into simpler models. It is indeed possible to compose an alternative model of the model B from a model-A element and a compliance element, as illustrated in Fig. 12(a). The same is true

$$\hat{\Phi}_Z(\mathbf{x}) = \begin{cases} \Phi(\mathbf{x}) + Z \frac{\|\Phi(\mathbf{x})\|}{\|\mathbf{x}\|} \left(\frac{\mathbf{x} \|\Phi(\mathbf{x})\|}{\|\mathbf{x}\|} - \Phi(\mathbf{x}) \right), & \text{if } \|\mathbf{x}/Z\| > \|\Phi(\mathbf{x})\| \\ \mathbf{x}/Z, & \text{if } \|\mathbf{x}/Z\| \leq \|\Phi(\mathbf{x})\|. \end{cases} \quad (59)$$

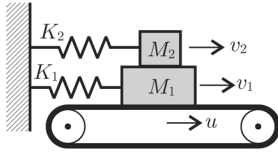


Fig. 9. Example of multiple frictional contacts.

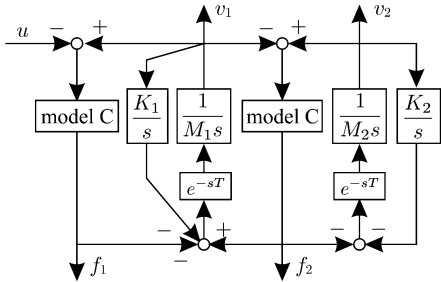


Fig. 10. Block diagram of the system of Fig. 9 using the model C.

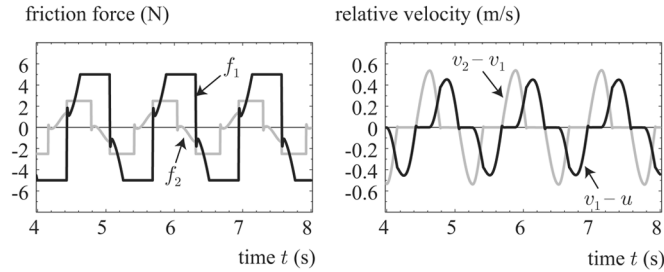


Fig. 11. Simulation of the system of Fig. 10; $u = 0.5 \sin(5t)$ m/s, $M_1 = M_2 = 1$ kg, $K_1 = 100$ N/m, $K_2 = 200$ N/m, $T = 0.001$ s. The first model-C element: $K = 3 \times 10^4$ N/m, $B = 300$ Ns/m, $\Phi(v) = F \text{sgn}(v)$, $F = 5$ N. The second model-C element: $K = 3 \times 10^4$ N/m, $B = 300$ Ns/m, $\Phi(v) = F \text{sgn}(v)$, $F = 2.5$ N.

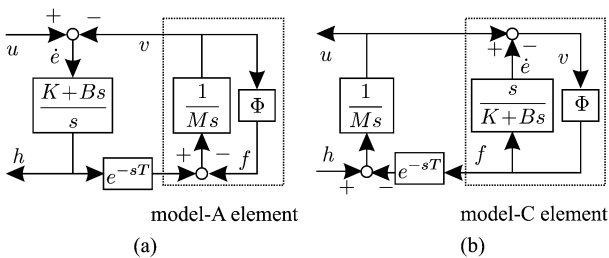


Fig. 12. Alternative model of the model B comprising (a) a model-A element, and (b) that of the model D comprising a model-C element.

with the model D, of which an alternative model can be composed of a model-C element and a mass element, as illustrated in Fig. 12(b). However, because these alternative models contain additional time delays compared with the “original” models (the models B and D in Fig. 3), they can become unstable with high stiffness or large timestep size.

Figs. 13 and 14 show simulation results demonstrating the difference between the original models and the alternative models. Fig. 13 shows the output force h from the original and the alternative of the model B when they are provided with a ramp velocity input. Fig. 14 shows the output velocity u from

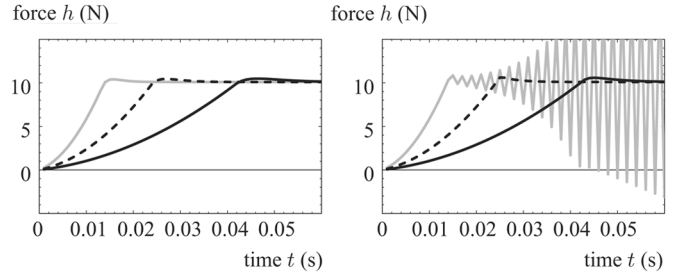


Fig. 13. Comparison of the model B (left) and its alternative model in Fig. 12(a) (right); $K = 8.3 \times 10^4$ N/m (gray), 2.5×10^5 N/m (dashed), and 7.5×10^5 N/m (black solid); input $u = 0.1t$ m/s; $M = 1$ kg, $B = 2\sqrt{K/M}$, $\Phi(v) = F \text{sgn}(v)$, $F = 10$ N, $T = 0.001$ s.

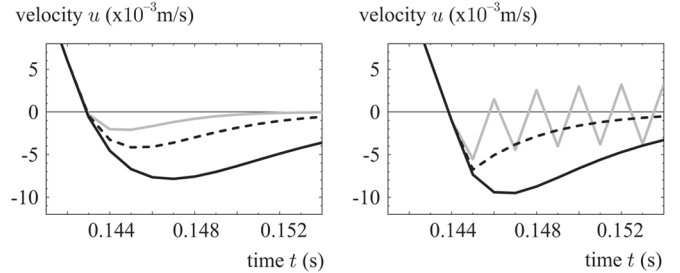


Fig. 14. Comparison of the model D (left) and its alternative model in Fig. 12(b) (right); $K = 8.3 \times 10^4$ N/m (gray), 2.5×10^5 N/m (dashed), and 7.5×10^5 N/m (black solid); initial condition $u = 1$ m/s and input $h = 0$ N; $M = 1$ kg, $B = 2\sqrt{K/M}$, $\Phi(v) = F \text{sgn}(v)$, $F = 7$ N, $T = 0.001$ s.

the original and the alternative of the model D when they are provided with a nonzero initial velocity and zero input force. These results show that the alternative models can become unstable or vibratory when the stiffness is chosen high, while the stiffness in the models B and D is not limited. Therefore, we can conclude that the models B and D can be better choices in some limited cases, due to their robustness against high stiffness and large timestep size.

C. Parameter Design for Model C

The model C can be used as a versatile element for simulating a frictional contact, but systems including model-C elements can become sensitive to the choice of parameter values, as demonstrated in Fig. 14. However, it does not exhibit either drift or chattering provided that the parameters K and B are properly chosen. The parameter design for the model C can be discussed in a common framework with conventional eigenvalue problems in finite difference equations.

Consider the system of Fig. 12(b) as an example. This system includes a model-C element and a mass element. Due to the mass element $1/(Ms)$, u_k is determined as follows:

$$u_k = u_{k-1} + (T/M)(h_k - f_{k-1}). \quad (60)$$

When the model-C element is in static friction, (38) reduces to the following:

$$f_k = (B + TK)u_k + Ke_{k-1} \quad (61)$$

$$e_k = e_{k-1} + Tu_k. \quad (62)$$

When $h_k = 0$, eliminating f_k and f_{k-1} from (60), (61), and (62) yields

$$\begin{bmatrix} e_k \\ u_k \end{bmatrix} = \begin{bmatrix} 1 - T^2 K/M & T - T^2 B/M \\ -TK/M & 1 - TB/M \end{bmatrix} \begin{bmatrix} e_{k-1} \\ u_{k-1} \end{bmatrix}. \quad (63)$$

To realize a nonoscillatory convergence in static friction, the eigenvalues of the 2-by-2 matrix in (63) need to be real numbers between 0 and 1. We can conclude that $T^2 < M/(4K)$ is necessary if B is chosen to realize critical damping, i.e., $B^2 = 4KM$. (The dashed curve in Fig. 14 (right) shows the marginal case, $T^2 = M/(4K)$.)

In more complicated situations, including multiple objects, parameter values may be chosen through trial and error. (This was the case for the simulation of Fig. 11.) The need for trial and error for parameter tuning is a common drawback of penalty-based simulations [23].

D. Controlling Haptic Interfaces

The admittance-type friction models, the models A and D, can be applied to haptic interfaces with force sensors. This application can be considered as a sort of admittance-control scheme. In this scheme, the force sensor measurements are provided as input to an admittance-type model, and the model produces position (or velocity) signal as output. The haptic interface is controlled so as to follow this position signal using position control. Using stiff position control servo can reduce the influence of the inertia and joint friction in the device. Thus, this scheme has been used effectively with relatively large haptic interfaces with hard nonlinearities [26], [27]. For haptic friction rendering using admittance-controlled devices, the model A will be preferred to the model D due to its simplicity, unless there is a specific need for compliance between the (virtual) sliding object and the (virtual) fixed surface. The application of the model A to an admittance-controlled device is demonstrated later in Section V-A.

It has been recognized that the admittance-control scheme is sensitive to the noise in the force measurement [28] because the time-integral of noise signal produces an unbounded positional drift. The simulated friction force realized by the model A can act as a deadband on the force measurement. This will be effective to reduce the influence of the electric noise from the force sensors and the physiological tremor of the user's hand.

The impedance-type models, the models B and C, are suitable for sufficiently backdrivable haptic interfaces, such as SensAble's PHANTOM devices. In this application, the velocity obtained by position sensors (such as optical encoders) is used as input to the model, and the output force is directly commanded to actuators. Backdrivability is necessary because these models require velocity input. The model C will be preferred to the model B due to its simplicity unless there is a need for a virtual mass pulled through the haptic interface. The application of the model C to haptic rendering is demonstrated later in Section V-B.

V. IMPLEMENTATION

We have implemented the 2-D versions of the proposed friction models to two different haptic interfaces. The model A, which is admittance-type, was used with a large robotic manipulator equipped with a force sensor. Because this device had

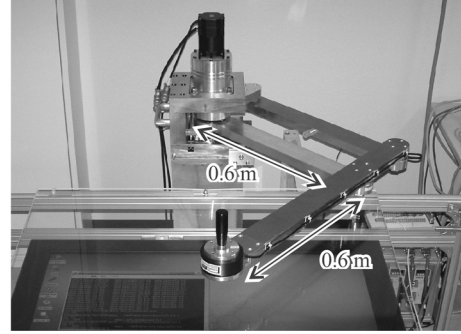


Fig. 15. Parallel-link manipulator in which the model A was implemented.

large joint friction and large link inertia, stiff position control servo was necessary. Thus, an admittance-type model was necessary for this device. The model C, which is impedance-type, was used with a force-feedback joystick having no force sensors. Because this device had sufficient backdrivability, the actuator torque was almost directly transmitted to the user's hand. Thus, an impedance-type model, which produces a force output, was suitable for this device.

We did not compare these two models on a common device. This is because such a comparison would require a haptic interface with both of a force sensor and sufficient backdrivability, which is uneconomical for practical use.

A. Admittance Control

The 2-D version of the model A, which is represented by (26), was implemented in the haptic interface shown in Fig. 15. It was a 2-degree-of-freedom (DOF) parallel link manipulator actuated by two AC servo motors with Harmonic drive gears. The joint friction was approximately 10 Nm for both joints. The joint angles were measured by optical encoders attached to the servo motors. A six-axis force sensor (Nitta IFS) was attached to the end-effector. This system was controlled by using a personal computer running ART-Linux. A handle grip attached to the force sensor was grasped and moved by an experimenter.

In the following, boldface symbols denote vectors. The friction force to be simulated was chosen as $\Phi(\mathbf{x}) = F\mathbf{x}/\|\mathbf{x}\|$ where $F = 6$ N, and the simulated mass in the model A was chosen as $M = 2$ kg. The timestep size (sampling interval) was $T = 0.001$ s. The input to the model A was the force measured by the force sensor \mathbf{h} , which is the force applied by the experimenter's hand. The output velocity \mathbf{v} from the model A was integrated into a position to be used as the desired position of the manipulator's end-effector. The end-effector's position was controlled to follow this desired position using stiff proportional-integral-derivative (PID) control on the joint angles.

The model A was demonstrated in a similar way to the experiment in [21]. The handle grip was moved along a trajectory that was chosen to demonstrate straight motions, curved motions, and static friction. Figs. 16 and 17 show the results. In Fig. 16, the thick curve represents the position trajectory of the end-effector measured by the optical encoders, and the thin line segments represent the force \mathbf{h} measured by the force sensor every 0.02 s. Fig. 17 shows the temporal changes in the measured position and the magnitude of the measured force, $\|\mathbf{h}\|$.

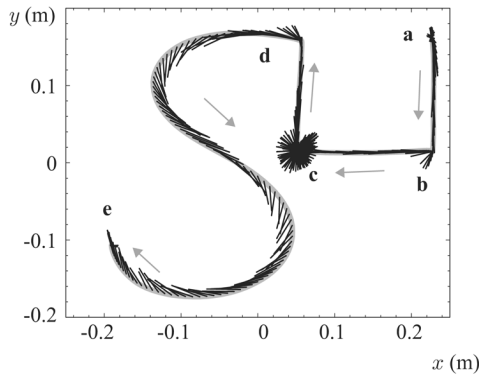


Fig. 16. Experimental results obtained from the model A; the measured position trajectory (gray thick lines) and force vectors \mathbf{h} measured by the force sensor (thin line segments).

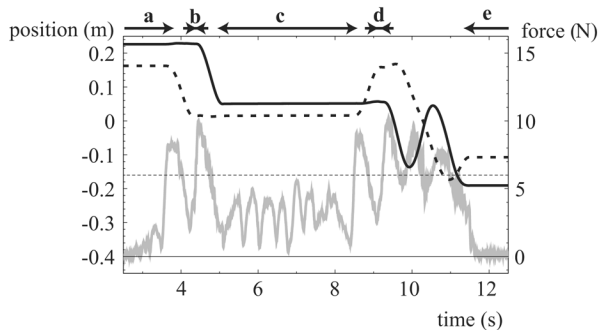


Fig. 17. Experimental results obtained from the model A; x (black solid) and y (black dashed) coordinates of the measured position and the magnitude of the force, $\|\mathbf{h}\|$, (gray) measured by the force sensor.

The lettered points in Fig. 16 and time periods in Fig. 17 correspond to each other.

Fig. 16 shows that during the straight motions (from a to d), the force measured by the force sensor is in the same direction of the motion. This indicates that the friction model A properly exhibits kinetic friction. At the point c, the end-effector is stationary. This is because, as is apparent from Fig. 17, the force from the experimenter's hand is smaller than the simulated friction force $F = 6$ N. This indicates that the model A properly exhibits static friction, and that it does not drift even under fluctuating external forces. In the curved motion from d to e, the experimenter's force resists the friction force and the centrifugal force caused by the simulated mass in the model. Thus, the force vectors are slanted to the inside of the curve.

The measured force \mathbf{h} cannot be attributed to the real friction in the manipulator's joints, but instead to the simulated friction produced by the proposed model. This is because the end-effector force caused by the joint friction would be anisotropic and dependent on the manipulator's configuration, while the force in Fig. 16 is isotropic and homogeneous. The joint friction torque is almost totally annihilated by the stiff PID control servo on joint angles.

It has been recognized that in admittance-type haptic rendering, the minimum simulated inertia depends on the actual dynamics of the haptic device, the architecture of the low-level position controller, and the firmness of the user's grasp [26],

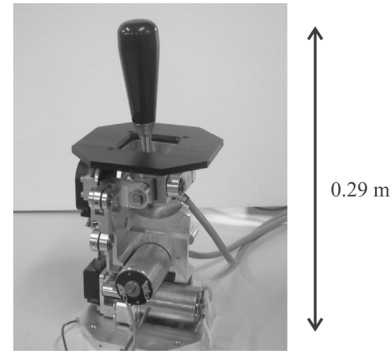


Fig. 18. Force-feedback joystick in which the model C was implemented.

[29]. In the literature, the minimum simulated inertia of some recent admittance-controlled haptic interfaces are reported to be around 2 kg or above [26], [29], [30]. We informally tried some values less than 2 kg for the simulated mass M , but it tended to produce oscillatory behavior during kinetic friction, especially with a firm grasp on the handle grip. A smaller value for M might be possible by a careful design of the joint angle controllers, but it is outside the scope of this paper.

B. Impedance Control

The 2-D version of the model C, which is represented by (38), was implemented in the setup shown in Fig. 18. It was a 2-DOF force-feedback joystick actuated by two DC servo motors. The position of the stick was measured by optical encoders attached to the motors. This device was backdrivable, and was not equipped with a force sensor. It was controlled by using a personal computer running ART-Linux. The joystick was moved by an experimenter's hand.

The velocity measured by the optical encoders was provided to the model C as the input velocity \mathbf{u} , and the output force \mathbf{f} was commanded to the motors. The friction force to be simulated was chosen as $\Phi(\mathbf{x}) = F\mathbf{x}/\|\mathbf{x}\|$ where $F = 4$ N. The timestep size (sampling interval) was $T = 0.001$ s, and the other parameters were chosen as $K = 6000$ N/m and $B = 10$ Ns/m.

This experiment was also performed in a way similar to the experiment in [21]. The tip of the joystick was moved by an experimenter to demonstrate straight motions, curved motions, and static friction. The results are shown in Figs. 19 and 20. The position data shown in the figures are those measured by the optical encoders, while the force data are the force command \mathbf{f} sent to the actuators. The force data in Fig. 19 are plotted every 0.01 s. The lettered points a–e in the two figures correspond to each other.

Fig. 19 shows that during the motions (a to b and b to d), the friction force is properly exerted in the opposite direction of the velocity. Unlike that in Fig. 16, the force opposes the velocity even in the curved motion (c to d) because the model C does not include a mass. Fig. 20 shows that, in the region b, the actuator force is fluctuating below the friction force $F = 4$ N due to a fluctuating force from the experimenter's hand. Even in this situation, the joystick is controlled to be maintained at a fixed point, without drift. This shows that the model C properly exhibits static friction.

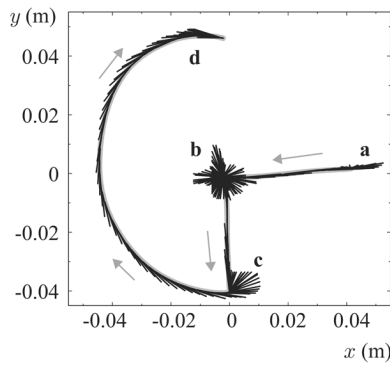


Fig. 19. Experimental results obtained from the model C; the measured position trajectory (gray thick lines) and force vectors \mathbf{f} commanded to the actuators (thin line segments).

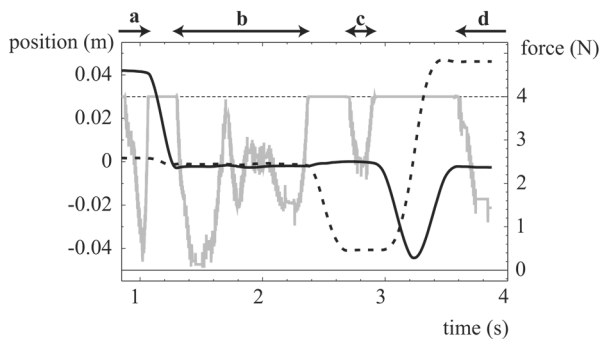


Fig. 20. Experimental results obtained from the model C; x (black solid lines) and y (black dashed lines) coordinates of the measured position and the magnitude of the force, $\|\mathbf{f}\|$, (gray) commanded to the actuators.

VI. CONCLUSION

We have presented a set of closed-form, discrete-time friction models (the models A, B, C, and D) for the purpose of haptic rendering. These friction models are derived from implicit Euler integration of Coulomb-like discontinuous friction and linear mass-spring-damper dynamics. These models include rate-dependent friction laws, and their extension to multidimensional cases is easy in most practical cases. The model D and its special case, the model A, are admittance-type models, while the model B and its special case, the model C, are impedance-type models. The models A and C will be practically useful for the purposes of haptic rendering and penalty-based simulations. The models B and D can be effective in some limited cases to maintain numerical stability. The admittance-type models are suitable for admittance-controlled haptic interfaces equipped with force sensors. The impedance-type models are suitable for sufficiently backdrivable haptic interfaces. The model C can be used as a versatile element representing a frictional contact between objects in penalty-based multibody simulations. The validity of the models was demonstrated through numerical examples and implementation experiments.

Future work will investigate the application of the proposed models to friction compensation, which will require accurate modeling of various features of real friction phenomena, such as hysteresis and lubricant dynamics. It has been known that a parallel connection of multiple elastoplastic element is effective for

describing hysteresis in mechanical systems [31]. Because an elastoplastic element can be represented by the model C in discrete time, a parallel connection of multiple model-C elements will be able to capture hysteresis in presliding displacement. Inclusion of higher order lubricant dynamics, such as frictional memory [11], will need further studies.

ACKNOWLEDGMENT

The authors thank the engineers at Toyota Motor Corporation who motivated and inspired their research.

REFERENCES

- [1] R. Kikuuwe, N. Takesue, A. Sano, H. Mochiyama, and H. Fujimoto, "Fixed-step friction simulation: From classical Coulomb model to modern continuous models," in *Proc. IEEE/RSJ Int. Conf. Intell. Robots Syst.*, 2005, pp. 3910–3917.
- [2] D. Karnopp, "Computer simulation of stick-slip friction in mechanical dynamic systems," *Trans. ASME: J. Dyn. Syst., Meas., Control*, vol. 107, no. 1, pp. 100–103, 1985.
- [3] C. Richard and M. R. Cutkosky, "Friction modeling and display in haptic applications involving user performance," in *Proc. IEEE Int. Conf. Robot. Autom.*, 2002, pp. 605–611.
- [4] S. E. Salcudean and T. Vlaar, "On the emulation of stiff walls and static friction with a magnetically levitated input-output device," *Trans. ASME: J. Dyn. Syst., Meas., Control*, vol. 119, pp. 127–132, 1997.
- [5] C. Richard, "On the identification and haptic display of friction," Ph.D. dissertation, Stanford Univ., Stanford, CA, 2000.
- [6] D. D. Quinn, "A new regularization of Coulomb friction," *Trans. ASME: J. Vib. Acoust.*, vol. 126, no. 3, pp. 391–397, 2004.
- [7] J. A. C. Martins and J. T. Oden, "A numerical analysis of a class of problems in elastodynamics with friction," *Comput. Methods Appl. Mech. Eng.*, vol. 40, no. 3, pp. 327–360, 1983.
- [8] A. Bonsignore, G. Ferretti, and G. Magnani, "Analytical formulation of the classical friction model for motion analysis and simulation," *Math. Comput. Model. Dyn. Syst.*, vol. 5, no. 1, pp. 43–54, 1999.
- [9] F. A. Tariku and R. J. Rogers, "Improved dynamic friction models for simulation of one-dimensional and two-dimensional stick-slip motion," *Trans. ASME: J. Tribol.*, vol. 123, no. 4, pp. 661–669, 2001.
- [10] A. F. Filippov, *Differential Equations with Discontinuous Righthand Sides*. Norwell, MA: Kluwer, 1988.
- [11] B. Armstrong-Hélouvy, P. Dupont, and C. Canudas de Wit, "A survey of models, analysis tools and compensation methods for the control of machines with friction," *Automatica*, vol. 30, no. 7, pp. 1083–1138, 1994.
- [12] P. R. Dahl, "A solid friction model," Aerospace Corp., Tech. Rep. TOR-0158(3107-18)-1, 1968.
- [13] C. Canudas de Wit, H. Olsson, K. J. Åström, and P. Lischinsky, "A new model for control of systems with friction," *IEEE Trans. Autom. Control*, vol. 40, no. 3, pp. 419–425, Mar. 1995.
- [14] J. Swevers, F. Al-Bender, C. G. Ganseman, and T. Prajogo, "An integrated friction model structure with improved presliding behavior for accurate friction compensation," *IEEE Trans. Autom. Control*, vol. 45, no. 4, pp. 675–686, Apr. 2000.
- [15] P. Dupont, V. Hayward, B. Armstrong, and F. Altpeter, "Single state elastoplastic friction models," *IEEE Trans. Autom. Control*, vol. 47, no. 5, pp. 787–792, May 2002.
- [16] V. Lampaert, J. Swevers, and F. Al-Bender, "A generalized Maxwell-slip friction model appropriate for control purposes," in *Proc. Int. Conf. Phys. Control*, 2003, pp. 1170–1177.
- [17] G. Ferretti, G. Magnani, and P. Rocco, "An integral friction model," in *Proc. IEEE Int. Conf. Robot. Autom.*, 2004, pp. 1809–1813.
- [18] —, "Modular dynamic modeling and simulation of grasping," in *Proc. IEEE/ASME Int. Conf. Adv. Intell. Mechatron.*, 1999, pp. 428–433.
- [19] E. Velenis, P. Tsiotras, and C. Canudas de Wit, "Extension of the LuGre dynamic tire friction model to 2D motion," in *Proc. 10th Mediterranean Conf. Control Autom.*, 2002, THA 5-3.
- [20] D. A. Haessig, Jr. and B. Friedland, "On the modeling and simulation of friction," *Trans. ASME: J. Dyn. Syst., Meas., Control*, vol. 113, pp. 354–362, 1991.
- [21] V. Hayward and B. Armstrong, "A new computational model of friction applied to haptic rendering," in *Experimental Robotics VI*. New York: Springer-Verlag, 2000, pp. 404–412.

- [22] S. Hasegawa, N. Fujii, Y. Koike, and M. Sato, "Real-time rigid body simulation based on volumetric penalty method," in *Proc. 11th Symp. Haptic Interfaces for Virtual Environ. Teleoperator Syst.*, 2003, pp. 326–332.
- [23] K. Erleben, J. Spurring, K. Henriksen, and H. Dohlmann, *Physics-Based Animation*. Boston, MA: Charles River Media, 2005.
- [24] Y. J. Lootsma, A. J. van der Schaft, and M. K. Çamblibel, "Uniqueness of solutions of linear relay systems," *Automatica*, vol. 35, pp. 467–478, 1999.
- [25] W. P. M. H. Heemels, M. K. Çamblibel, and J. M. Schumacher, "A time-stepping method for relay systems," in *Proc. 39th IEEE Conf. Decision Control*, 2000, pp. 4461–4466.
- [26] R. Q. Van Der Linde and P. Lammertse, "HapticMaster—A generic force controlled robot for human interaction," *Ind. Robot*, vol. 30, no. 6, pp. 515–524, 2003.
- [27] M. Ueberle, N. Mock, and M. Buss, "VISHARD10, a novel hyper-redundant haptic interface," in *Proc. 12th Symp. Haptic Interfaces for Virtual Environ. Teleoperator Syst.*, 2004, pp. 58–65.
- [28] J. J. Abbott, G. D. Hager, and A. M. Okamura, "Steady-hand teleoperation with virtual fixtures," in *Proc. 12th IEEE Int. Workshop Robot and Human Interactive Commun.*, 2003, pp. 145–151.
- [29] M. Ueberle and M. Buss, "Control of kinesthetic haptic interfaces," in *Proc. Workshop on Touch and Haptics, IEEE/RSJ Int. Conf. Intell. Robots Syst.*, 2004, pp. 1–14.
- [30] E. de Vlugt, A. C. Schouten, F. C. T. van der Helm, P. C. Teerhuis, and G. G. Brouwn, "A force-controlled planar haptic device for movement control analysis of the human arm," *J. Neurosci. Meth.*, vol. 129, no. 2, pp. 151–168, 2003.
- [31] W. D. Iwan, "A distributed-element model for hysteresis and its steady-state dynamic response," *Trans. ASME: J. Appl. Mech.*, vol. 33, no. 4, pp. 893–900, 1966.



Ryo Kikuuwe (S'02–M'03) received the B.S. and M.S. degrees in mechanical engineering in 1998 and 2000, respectively, and the Ph.D.(Eng.) degree in mechanical engineering in 2003, all from Kyoto University, Kyoto, Japan.

Currently he is a Research Associate with the Nagoya Institute of Technology, Nagoya, Japan. His research interests include human-robot coordination, haptic rendering, discrete-time simulations, and tactile sensing.

Dr. Kikuuwe is a member of the Robotics Society of Japan, the Japan Society of Mechanical Engineers, and the Society of Instrument and Control Engineers (Japan).



Naoyuki Takesue (M'02) received the B.E. and M.E. degrees in mechanical and control engineering from the University of Electro-Communications, Tokyo, Japan, in 1995 and 1997, respectively, and the Ph.D. (engineering) degree from Osaka University, Osaka, Japan, in 2000.

From 1997 to 2000, he was a Research Fellow of the Japan Society for the Promotion of Science. He was a Research Associate with Osaka University from April 2000 to March 2003. He is currently an Associate Professor with Nagoya Institute of

Technology, Nagoya, Japan. His research interests include motion control of mechanical systems, mechatronics systems using ER/MR fluid, human-machine interface, haptics, and touch technology.



Akihito Sano received the B.S. and M.S. degrees in precision engineering from Gifu University, Gifu, Japan, in 1985 and 1987, respectively, and the Ph.D. (Eng.) degree from Nagoya University, Nagoya, Japan, in 1992.

He is currently a Professor with the Department of Engineering Physics, Electronics and Mechanics, Nagoya Institute of Technology, Nagoya, Japan. His research interest includes human-centered robotics, haptics and haptic interface, and passive walking.

Dr. Sano is a Fellow of the Japan Society of Mechanical Engineers. He received the Best Paper Award for a paper presented at the 2000 Japan-USA Symposium on Flexible Automation, and the Best Technical Exhibition Award in the 2004 First IEEE Technical Exhibition Based Conference on Robotics and Automation.



Hiromi Mochiyama (S'96–M'98) received the B.E. and M.E. degrees in electrical engineering in 1993 and 1995, respectively, from Waseda University, Tokyo, Japan, and the Ph.D. degree in information science in 1998 from the Japan Advanced Institute of Science and Technology, Hokuriku, Japan.

He is currently an Associate Professor with Nagoya Institute of Technology, Nagoya, Japan. His research interest includes haptics and robotic manipulation.



Hideo Fujimoto received the B.M.E. degree from Nagoya University, Nagoya, Japan, in 1970.

He is currently a Professor at the Graduate School, Nagoya Institute of Technology, Nagoya, Japan, and also the Director of the Quality Innovation Techno-Center, Nagoya, Japan. He is a Doctor of Engineering. His main research interests are production system, intelligent robot, virtual reality, and sensitive engineering.

Prof. Fujimoto is a Fellow of the Japan Society of Mechanical Engineers, a Standing Director and the Council Chair of the Society of Instrument and Control Engineers, and the President of Scheduling Society of Japan. He received the Best Paper Award for a paper presented at the Japan-USA Flexible Automation Symposium 2000, the Best Paper Award at the 6th Robotics Symposium, the Contribution Award from the SI Section, Society of Instrument and Control Engineers, and the Great Contribution Award from the Production System Section, Japan Society of Mechanical Engineers in 2002.